Archaeological Discovery, 2024, 12, 66-81
https://www.scirp.org/journal/ad
ISSN Online: 2331-1967
ISSN Print: 2331-1959

Iron-Rich Red Clays on the Turin Shroud: Optical Microscopy Studies and SEM-EDX Analyses

Gérard Lucotte[1*], Thierry Thomasset[2], Thierry Deroin[3]

[1]Institute of Molecular Anthropology, Paris, France
[2]Laboratory of Physico-Chemical Analysis, UST of Compiègne, Compiègne, France
[3]Department of Phanerogamy, Natural History Museum of Paris, Paris, France
Email: *lucottegerard@outlook.fr

How to cite this paper: Lucotte, G., Thomasset, T., & Deroin, T. (2024). Iron-Rich Red Clays on the Turin Shroud: Optical Microscopy Studies and SEM-EDX Analyses. *Archaeological Discovery, 12,* 66-81.
https://doi.org/10.4236/ad.2024.121004

Received: November 21, 2023
Accepted: January 21, 2024
Published: January 24, 2024

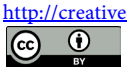

Abstract

We have explored by optical microscopy and scanning electrons microscopy coupled with energy dispersive X-ray fifteen particles located in a sample of the Face area of the Turin Shroud. They have the following peculiarities: they are alumino-silicate clays, with an elevated content (up to 56%) of iron; their sides are comprised between 1.5 µm and 19 µm; their forms are rounded or more elongated, but more often with angular outlines. When observable, their colours are red or red-brown. All these particles have a little quantity of the phosphorous element (up to 5%) in their compositions. The biggest ones show some morphological heterogeneity on their surfaces, suggesting that they are chipboards of some micro-organisms.

Keywords

Turin Shroud, Face Area, Red Clays, Optical Microscopy, Scanning Electron Microscopy, Energy Dispersive X-Ray

1. Introduction

The Turin Shroud (TS), the most important Christ's relic, is a well known object in which a body image is imprinted. Numerous scientific approaches were realized concerning this precious relic (Marion & Lucotte, 2006). We have obtained a small triangular sticky tape that was sample d on its surface (corresponding to the Face of this body) and we concentrated in the past years on the study of microscopic organic structures located on the surface of this sticky tape, including: linen fibers (Lucotte, 2015a), pollens and spores (Lucotte, 2015b), red blood cells (Lucotte, 2015c), skin debris (Lucotte, 2016), an hair fragment (Lucotte &

Thomasset, 2017a) and osseous remains (Lucotte & Thomasset, 2017b). More recently, we published gold and silver particles (Lucotte, 2022a), and lapis lazuli particles (Lucotte & Thomasset, 2023), detected on the surface of the triangle.

In a preliminary analysis (Lucotte, 2012), we studied some particles, notably the b8 and the ei4 particles, that seems to look like (by their morphologies and sizes) to red blood cells; they are in fact some peculiar clays (Lucotte, 2022b), with elevated values of iron oxide in their compositions, that conferring to it the red colour observed in optical microscopy.

In the present study, for obtaining precisions about these peculiar red clays, we observe and characterize in details the clay particles (including b8 and i4) located on the surface of the triangle, presenting such similar peculiarities. A total number of fifteen particles were so detected.

2. Material and Methods

The material is a small (1.36 mm height, 614 µm wide) sticky tape triangle at the surface of which all particles were deposited. For practical reasons, the surface of this triangle was subdivided in 19 (named A to S) sub-samples areas (Lucotte, 2017). The positions of each particle sticking to the triangle surface were located in a double system of coordinates (in 186 adjacent squares of 50 × 50 µm). Particles of the sample were observed, with any preparation, on the adherent part of the triangle surface. All the particles described here were studied by optical microscopy and by SEM (Scanning Electron Microscopy)-EDX (Energy Dispersive X-ray) analysis.

Most of the particles studied were first observed by optical microscopy using a photo-microscope Zeiss, model III, 1972. The corresponding photographs were named as direct when they correspond to those studied by SEM-EDX, and as inverse hen it is the other side of the triangle that was observed.

Two SEM apparatus (SEM1 and SEM2) were used; both are Environmental versions: 1/A Philips XL. 30 instrument. GSE (Gaseous Secondary Electrons) and BSE (Back Scattered Electrons) procedures were used, the last one permitting the detection of heavy elements. 2/A FEI model Quanta 25 of FEG, both in LFD (Large Field Detector) and CBS (Circular Back Scattering) procedures.

Elemental analysis for each particle were realized by EDX, the SEM1 apparatus being equipped with a Bruker probe AXS-EDX and the SEM2 apparatus with a probe model X-flash 6/30. Each elemental analysis is given in the form of a spectrum, with kiloelectrons/Volts (ke/V) on the abscissa and elemental peak heights in ordinates. Highly resolutive (HR) spectra are those where the ordinate scale is in logarithms, for a better distinction of little peaks.

Normal compositions in elements are those where carbon and oxygen are not taken in consideration.

3. Results

The enlarged (about 1200×) optical view of **Figure 1** shows the right part of the B area of the triangle. Three red particles are visible in this view: the b8 particle

and the b 24 and b25 (red-brown) particles. Adjacent particles b24 and b25 are located to the left part of b22, which is a golden particle (Lucotte, 2015a).

The SEM1 photograph of **Figure 2** shows the b8 particle. It is a rounded particle of a maximal diameter of about 12 μm. Because of its form and colour, it mimics red blood cells (Lucotte, 2015c). There are three deposits at the b8 surface: a triangular Diatom, and two micro-filaments of titanium (Ti). The b8 surface is not smooth, and shows some evidence of micro-heterogeneity.

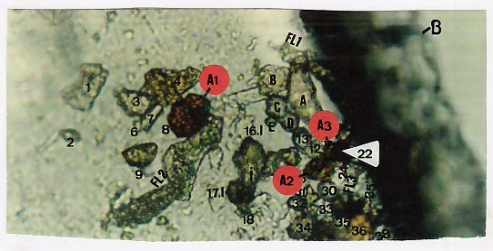

Figure 1. Optical view (1200×) of some part of the B area, showing the three particles A1 (b8), A2 (b25) and A3 (b24); b22 is a particle of gold alloy. B: the right border of the B area.

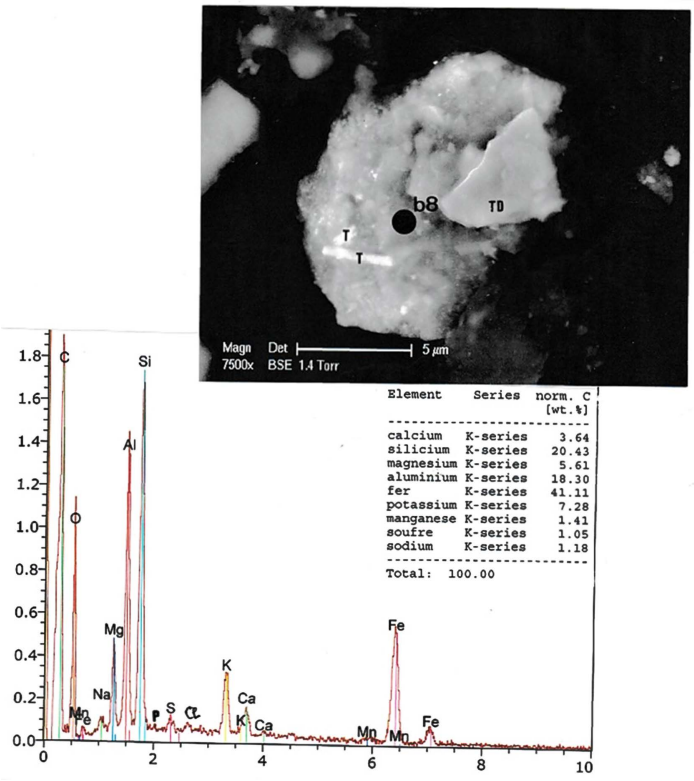

Figure 2. The b8 particle. *Above*: SEM1 photograph (7500×), in BSE, of the b8 particle. T: two titanium micro-filaments; TD: a Triangular Diatom. The big dot in the b8 center indicates the approximate area of the particle where EDX analysis is realized. *Below*: the b8 spectrum. C: carbon; O: oxygen; Fe (three peaks): iron; Na: sodium; Mg: magnesium; Al: aluminium; Si: silicium; P (traces): phosphorous. S: sulphur; Cl chlorine; K (two peaks): potassium; Ca (two peaks): calcium; Mn (traces): manganese. *Insert*: the normal composition (in wt. %) in elements of b8 (fer: iron; soufre: sulphur).

The b8 spectrum shows that it is a typical clay: the silicium (Si), the aluminium (Al) and the magnesium (Mg) peaks are in order of decreasing heights; there is potassium (K) and calcium (Ca). It is an iron-rich clay, because the iron (Fe) value is of about 41% and there are traces of manganese (Mn), attesting the "mineral" nature of the iron. There are little peaks of sodium (Na), of sulphur (S) and of chlorine (Cl) and also some traces of phosphorous (P).

The SEM1 photograph of Figure 3 shows the b24 particle, which is with hexagonal outlines and has a maximal measurement of about 6 µm. It is a clay, with an important main peak of iron; it has phosphorous and sulphur traces. This particle is contaminated by the gold (Au) of the b22 particle.

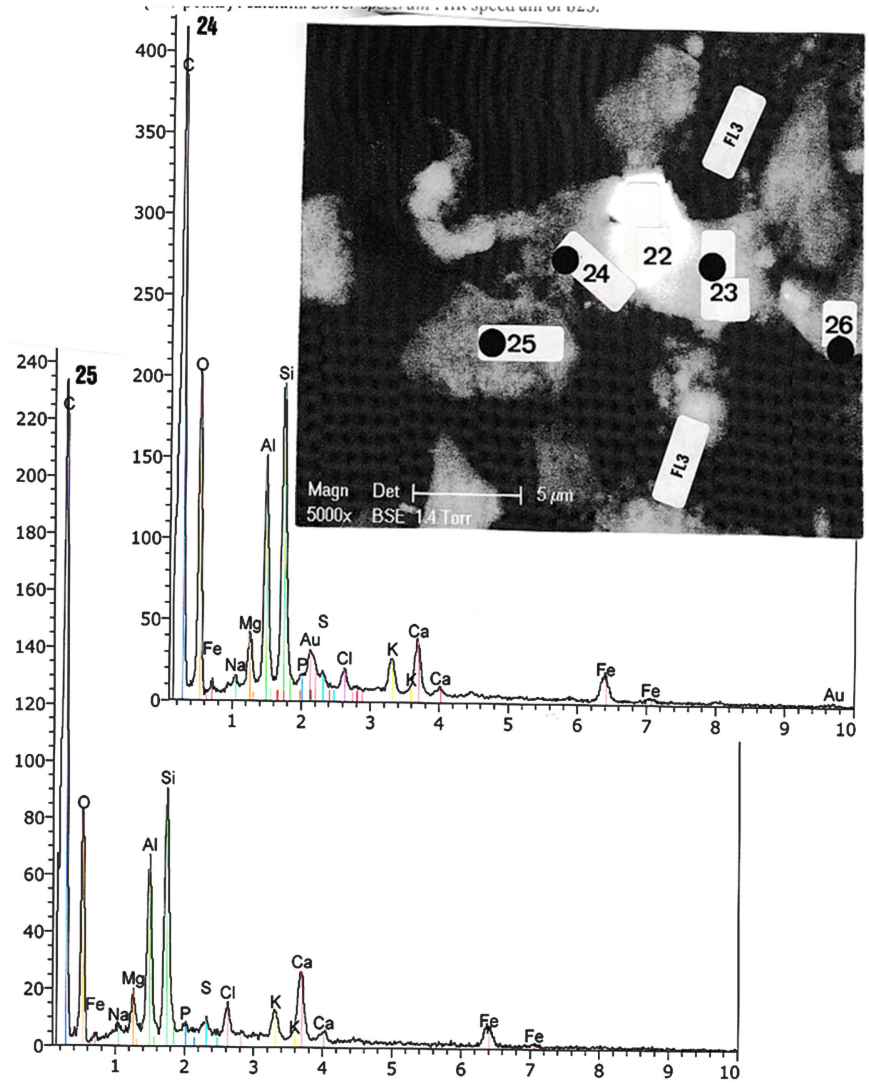

Figure 3. *Above*: SEM1 photograph (5000×), in BSE, showing particles b25, b24, b22, b23 and b26. FL3 are two parts of the linen fiber 3. *Upper spectrum*: HR spectrum of the b24 particle. C: carbon; O: oxygen; Fe (three peaks): iron; Na: sodium; Mg: magnesium; Al: aluminium; Si: silicium; P (traces): phosphorous; Au (two peaks): gold; S: sulphur; Cl: chlorine; K (two peaks): potassium; Ca (two peaks): calcium. *Lower spectrum*: HR spectrum of b25.

Similarly the b25 particle is also with hexagonal outlines, with a maximal measurement of 6.5 μm. It is also a clay, with an important mean peak of iron and little phosphorous and sulphur peaks.

Because of the proximity of b23 and b26 particles with the right border of the B area, we cannot see their colours in optical microscopy. They are two particles with hexagonal outlines, and with maximal sizes of 6 μm and 5.5 μm, respectively.

The b23 spectrum (Figure 4) is that of a clay with an elevated mean peak of iron, and phosphorous and sulphur traces. This particle is contaminated by the gold of b22. The b26 spectrum is also that of a clay with an elevated main peak of iron, and little peaks of phosphorous and sulphur.

Because of the proximity of a25 and a27 particles with the right border of the A area (Figure 5), we cannot see their colours. The a25 particle is with pentagonal outlines and of 6.5 μm of size; its spectrum is that of a clay with an important mean peak of iron, and with phosphorous and sulphur traces. The a27 particle is a little (3 μm) rounded particle; its spectrum is also that of an illite, with an important mean peak of iron and with phosphorous and sulphur little peaks (it is contaminated by titanium).

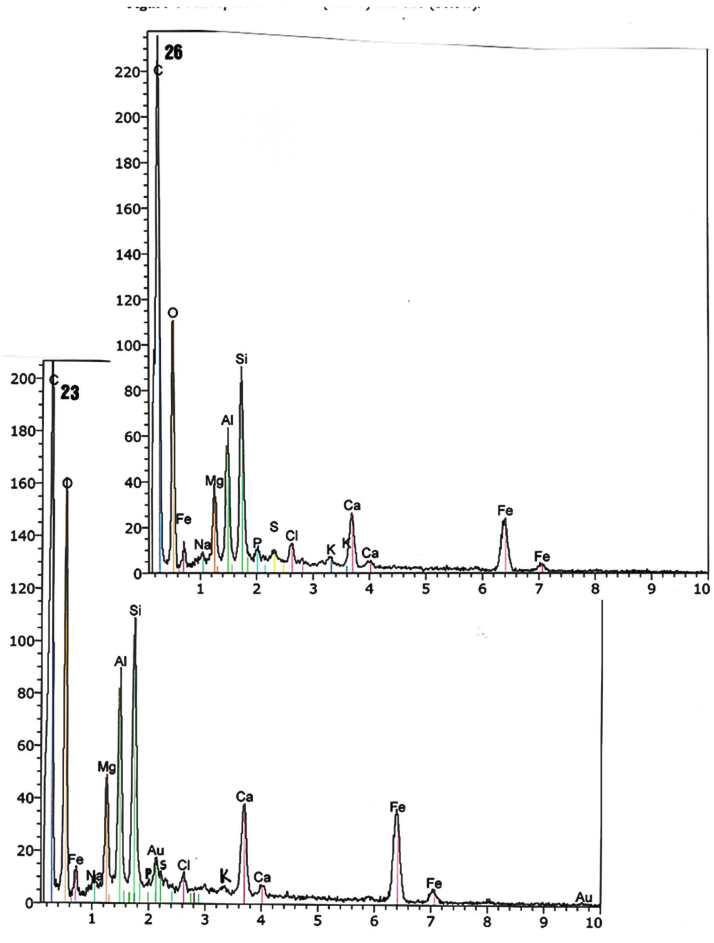

Figure 4. HR spectrum of b26 (above) and b23 (below).

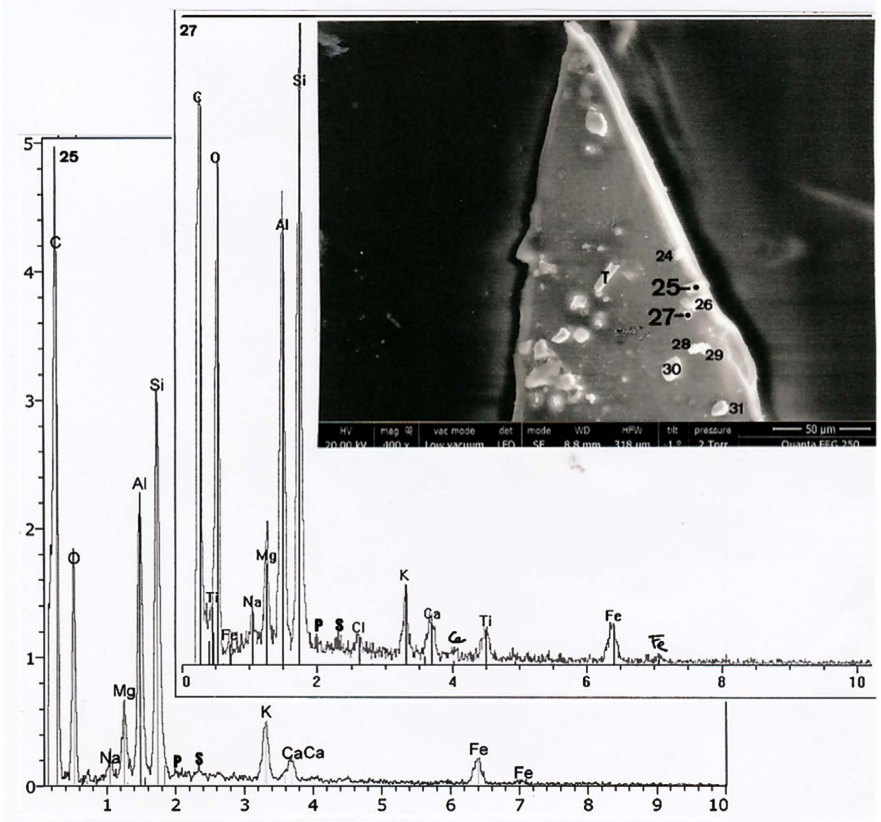

Figure 5. The a25 and a27 particles. *Above*: SEM2 photograph (400×), in LFD, the upper part of the A area, showing particles a25 and a27. (T is a titanium micro-filament). *Upper spectrum*: HD spectrum of a27. C: carbon; Ti (two peaks): titanium; Fe (three peaks): iron; Na: sodium; Mg: magnesium; Al: aluminium; Si: silicium. P: phosphorous; S: sulphur; Cl: chlorine; K: potassium; Ca (two peaks): calcium; *Lower spectrum*: HD spectrum of a25.

The optical photograph of Figure 6 of the lower part of the A area shows that the a41 particle is of a red-brown colour. It is a pentagonal particle of 5.5 μm of size; its spectrum is that of a clay with an elevated mean peak of iron. It has an important peak of phosphorous and a little peak of sulphur.

The SEM2 photograph of Figure 7 shows, in the right part of the G area, the g27, g30 and g33 particles; g27 is in fact (see the SEM photograph of Figure 8) a complex particle, constituted of at least seven parts (**1** - **7**). Its maximal length is of about 18 μm. The g30 particle is of small size (about 3.5 μm) and with a triangular form, but careful examination (see Figure 8) shows that it is driven under part 6 of g 27, and so must be of greater size. The g33 particle is squared in form, with a maximal size of 10.5 μm. These three particles are covered by very fine deposits of calcium carbonate micro-grains.

The inverted optical view of Figure 7 shows that the g27, g30 and g33 particles are of red-brown colours.

Figure 8 shows the g27 spectrum, that is of a clay with an elevated mean peak of iron; it has little peaks of phosphorous and sulphur. This spectrum shows an elevated value of the main calcium peak.

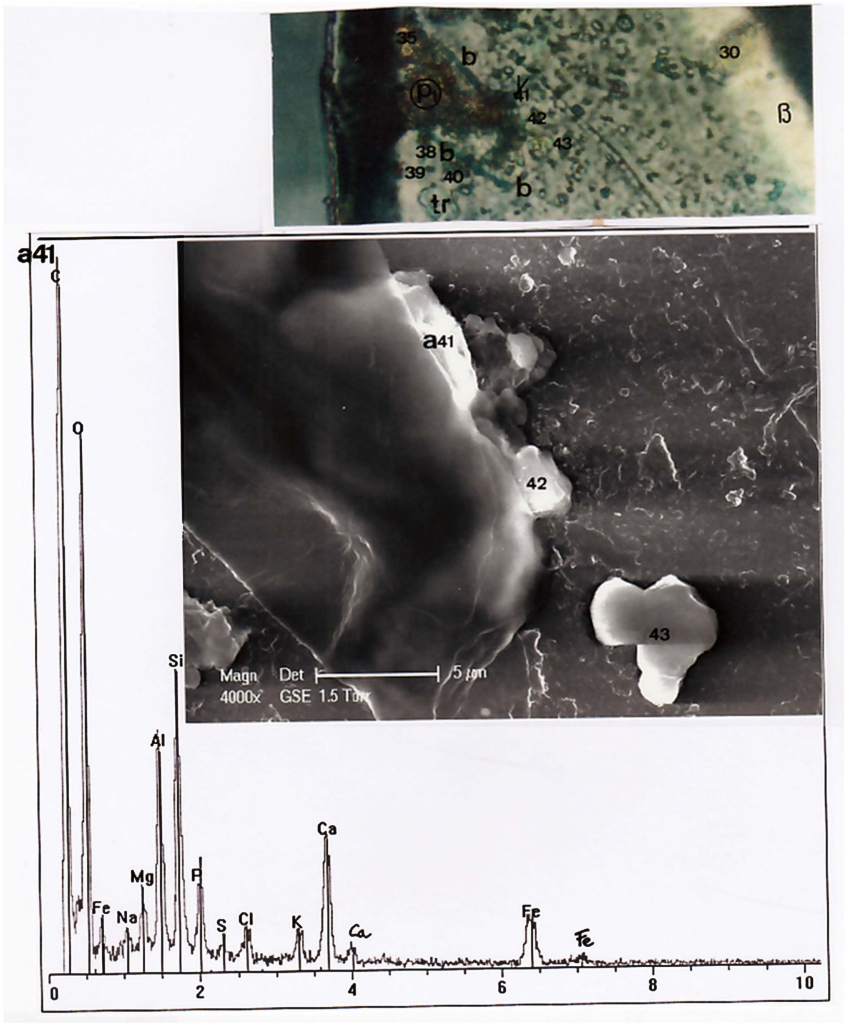

Figure 6. The a41 particle. *Above photograph*: optical view (1200×) of the left part of the low A area, showing the a41 particle (arrow point). P1 is a triangular fold of PVC plastic in this area part (B is the right border of the A area). *Below photograph*: SEM1 photograph (4000×) in GSE, showing the emerging part of the a41 particle (a42 is a glass and a43 a trilobed calcium carbonate). *Below*: the HR a41 spectrum. C: carbon; O: oxygen; Fe (three peaks): iron; Na: sodium; Mg: magnesium; Al: aluminium; Si: silicium; P: phosphorous; S: sulphur; K: potassium; Ca (two peaks): calcium.

Figure 9 shows the spectra of the g30 and g33 particles. Both are those of a clay with important main peaks of iron. The two spectra have peaks of phosphorous and sulphur, and elevated values of the main calcium peaks.

The inverted optical view of Figure 10 shows, in the right part of the I area, the red-brown colour of the i4 particle. The SEM1 photograph of Figure 10 shows that it is an elongated particle, with at least 9.5 µm of size. Careful examination of its surface permits to see that it is entirely constituted of some forms of micro-organisms of characteristic patterns.

The i4 spectrum is that of a clay, with an important peak of iron; it has little peaks of phosphorous and sulphur. It shows an elevated value of the main calcium peak, and traces of copper (Cu).

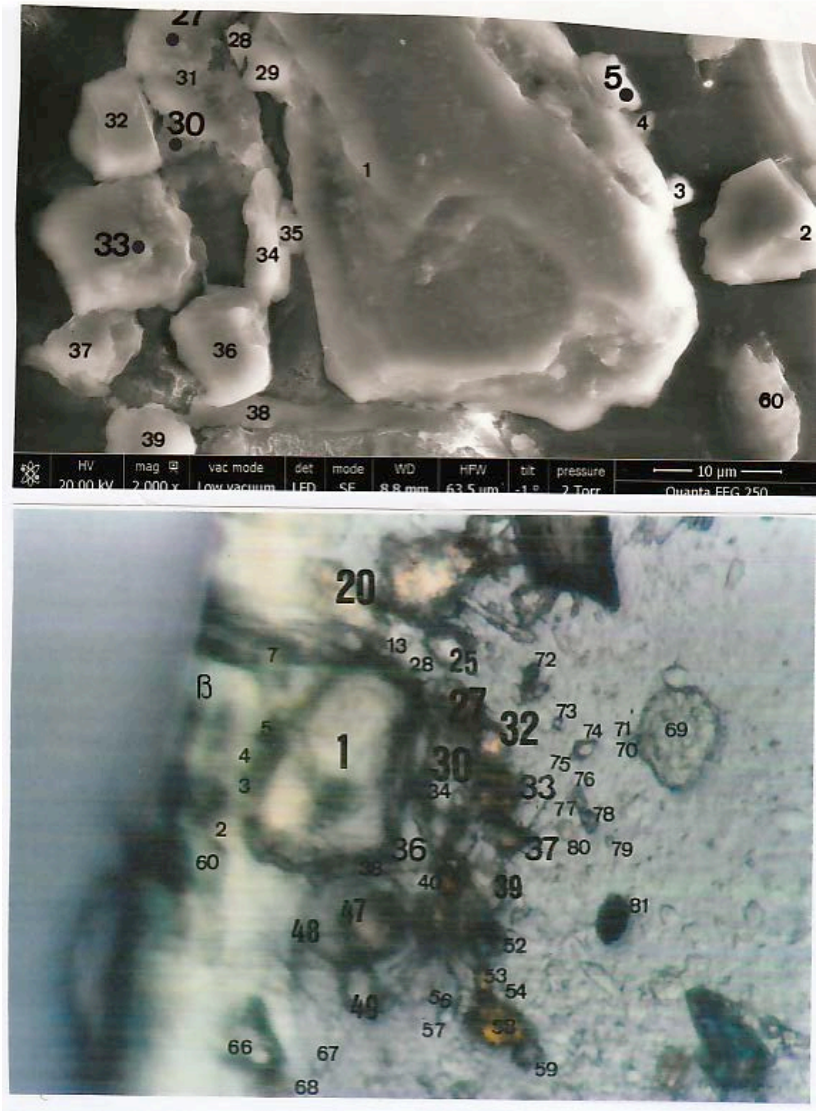

Figure 7. The g27, g30 and g33 particles. *Above*: SEM 2 photograph (2000×), in LFD, of some part of the G area (showing the different particles that surround the great g1 particle, which is a peridot), where particles g27, g30 and g33 are indicated in capital numbers (g28 is a glass; g29 is a calcium carbonate; g31 indicates fine deposits on g27 and g30; g32 is a dolomite; g34 is a biotite; g35 is a calcite; g36 is a silica; g37 is a phosphorite; g38 is the basal part of a silk fiber; g39 is a silica). *Below*: inverted optical view (1200×) of some part of the G area showing particles located at the left part of the g1 particle (a peridot), g27, g30 and g33 particles are indicated in capital numbers. (B Is the right border of the G area).

The SEM1 photograph of **Figure 11**, of a left part of the J area, shows the j50 and j51 particles. The j50 particle, detached from j51, is a little (1.5 µm) squared particle. Its spectrum is that of a clay, with an iron content of about 60%. It has a little peak of phosphorous. The j51 particle is elongated, with 7.5 µm of maximal length. There is also some evidence of micro-organisms on its surface. Its spectrum is that of a clay, with an elevated value of the main peak of iron; it has a little peak of phosphorous.

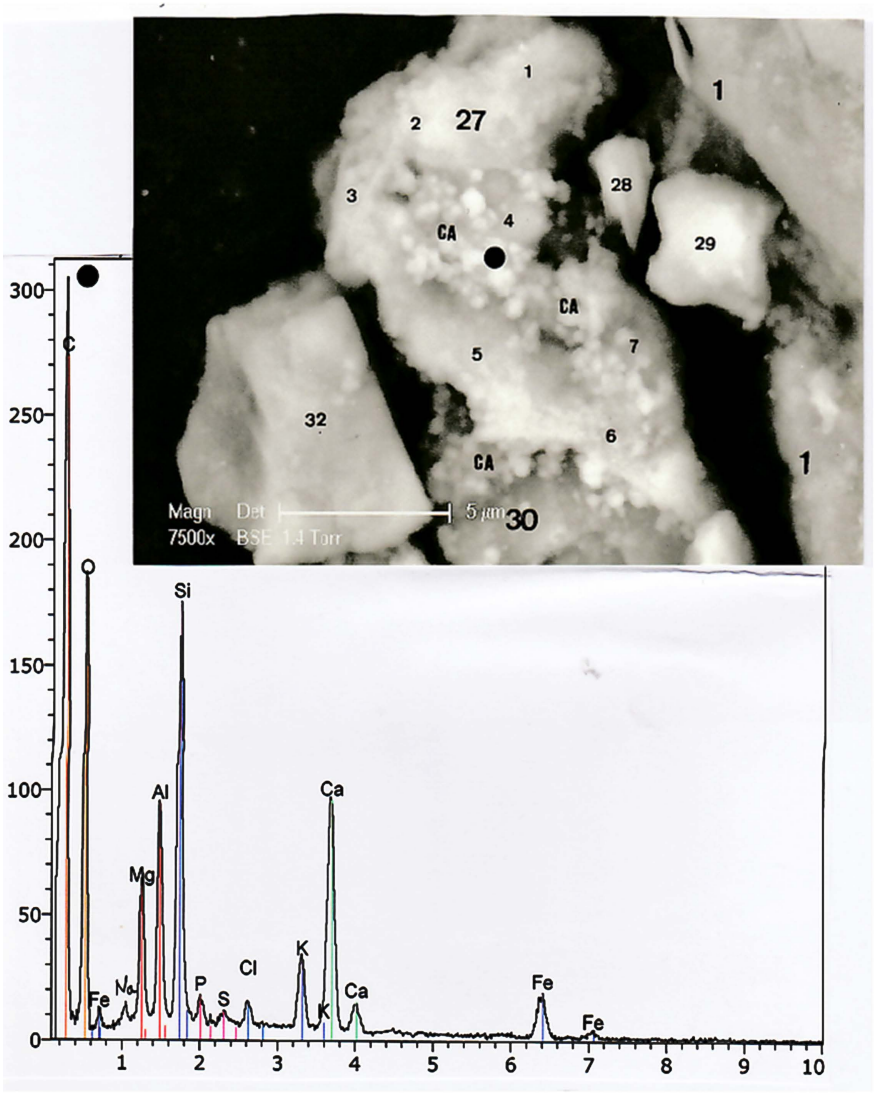

Figure 8. The g27 particle. *Above*: SEM1 photograph (7500×), in BSE, showing the g27 particle (covered, as the g30 particle, by a fine deposit of calcium carbonate: Ca). This complex is compounded of at least seven parts (numbered 1 to 7); the black point indicates the g27 region where EDX analysis is realized. *Below*: the HR spectrum of g27. C: carbon; O: oxygen; Fe (three peaks): iron; Na: sodium; Mg: magnesium; Al: aluminium; Si: silicium; P: phosphorous; S: sulphur; Cl: chlorine; K (two peaks): potassium; Ca (two peaks, with a major one): calcium.

Because of the proximity of j50 and j51 particles with left border of the J area, it is difficult to see their colours. Careful examinations of some optical views of the region shows however one yellow-red spot corresponding to the j50 particle, and a pale-red spot corresponding to the j51 particle.

The inverted optical photograph of Figure 12 shows, in the central part of the L area, the red colour of the l11 particle. The SEM photograph of that figure shows that l11 is an elongated complex particle, of a maximal length of 9 µm, constituted of at least three parts (**1**, **2** and **3**). There is also evidence of micro-organisms on its surface.

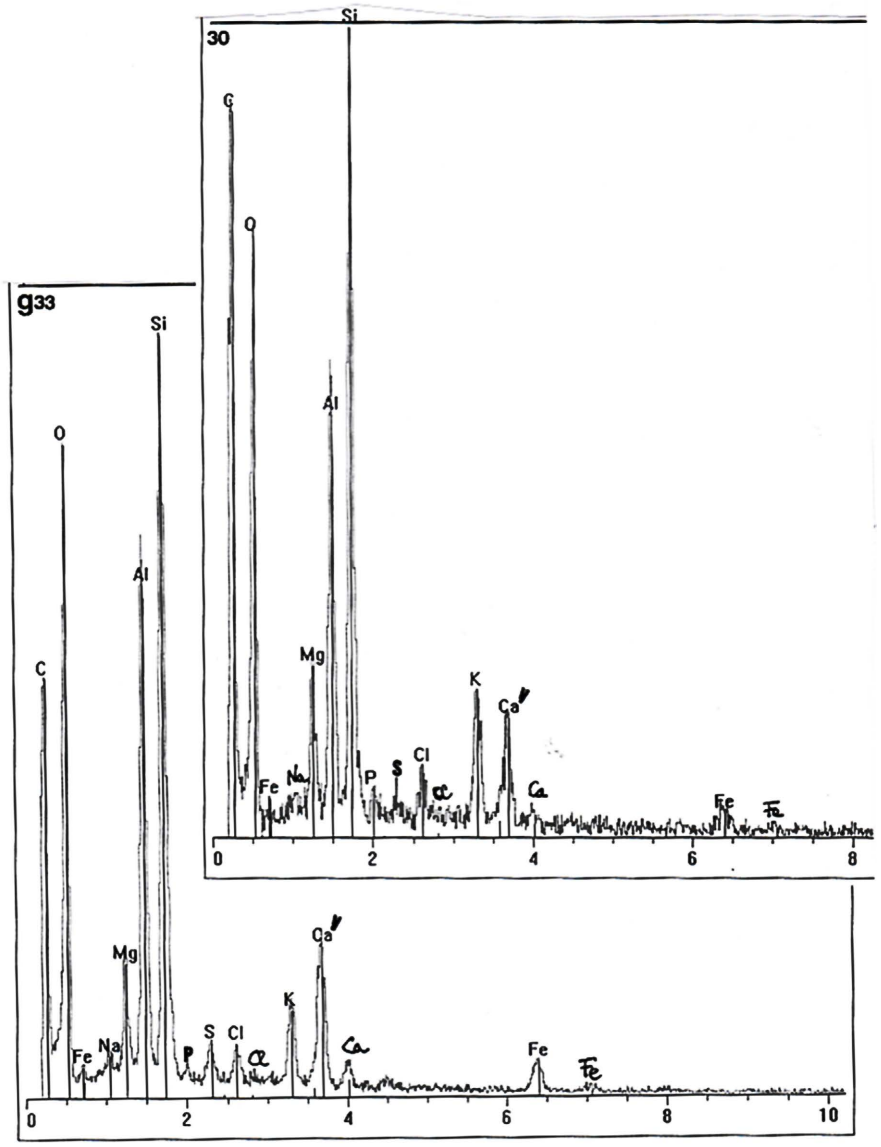

Figure 9. HR spectrum of the g30 (above) and g33 (below) particles. C: carbon; O: oxygen; Fe (three peaks): iron; Na: sodium; Mg: magnesium; Al: aluminium; Si: silicium; P: phosphorous; S: sulphur; Cl (two peaks): chlorine; K: potassium; Ca (two peaks): calcium (the arrow points indicate calcium carbonate contamination).

The l11 spectrum is that of a clay, with an iron value of about 56%. It has a great peak of phosphorous (of value of about 5%) and a smaller peak of sulphur (of a value of about 2%); the value of chlorine (about 6%) is also relatively elevated.

4. Discussion

Table 1 lists and characterizes the fifteen (three in the A area: a25, a27 and a41; five in the B area: b8, b23, b23 and b24, b25 and b26; three in the G area: g27, g30 and g33; one in the I area: i4; two in the J area: j50 and j51; one in the L area: l11) iron-rich clay particles detected in the various areas of the triangle. All have

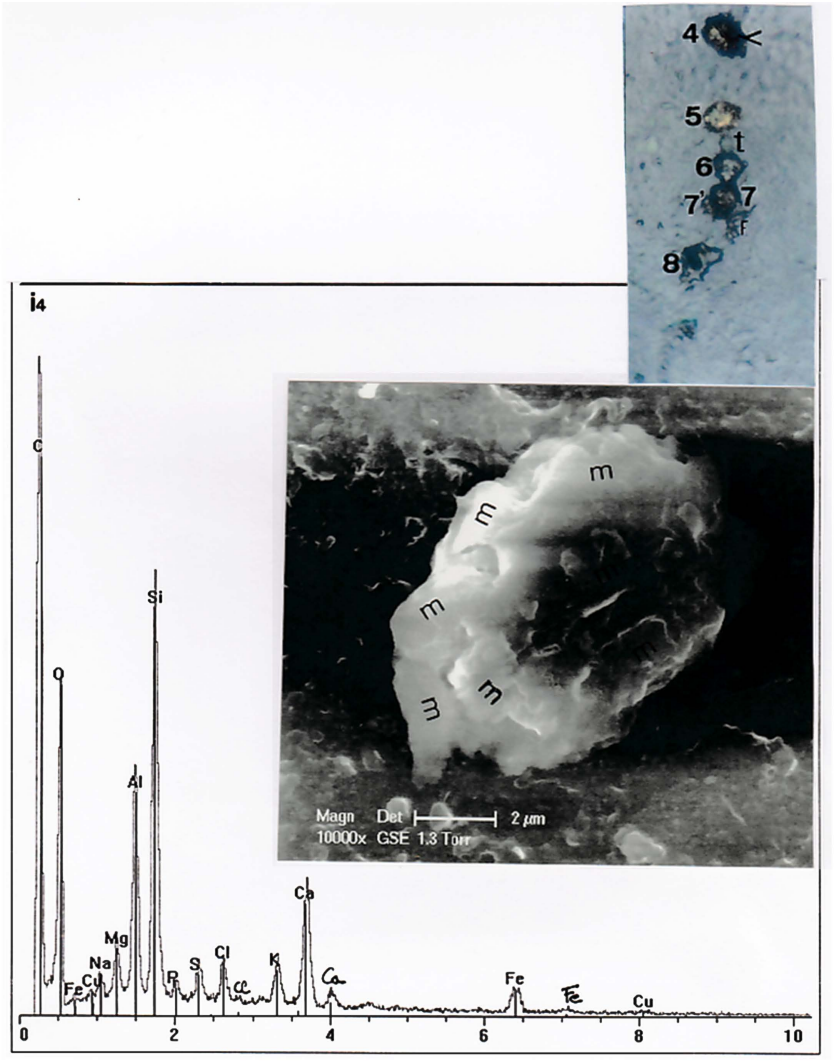

Figure 10. The i4 particle. *Upper photograph*: inverted optical view (1200×) of the right part of the I area showing the i4 particle (arrow point). *Lower photograph*: SEM1 photograph (10,000×), in GSE, of the i4 particle (m: micro-organisms). *Below*: the i4 spectrum. C: carbon; O: oxygen; Fe (three peaks): iron; Cu (two peaks): copper; Na: sodium; Mg: magnesium; Al: aluminium; Si: silicium; P: phosphorous; S: sulphur; Cl (two peaks): chlorine; K: potassium.

spectra of typical clays, with elevated iron-values; the iron oxide conferring a red colour, all these (when observable in optical microscopy) particles are of red-brown or red colour. So these iron-rich clays participate, together with those of hematite, biotite and cinnabar already detected (Lucotte et al., 2016), to the observed reddish tint of the triangle (Lucotte, 2017).

These iron-rich clays are of some interest for understanding the origin of the TS, because the soil of Mt. Sion (in Jerusalem) contains some red illites with quasi-similar spectra (Fanti et al., 2015). However more accurate analyses are necessary for a complete identification of these minerals, which are very similar to the clays of other Mediterranean areas influences by the winds of the Sahara desert.

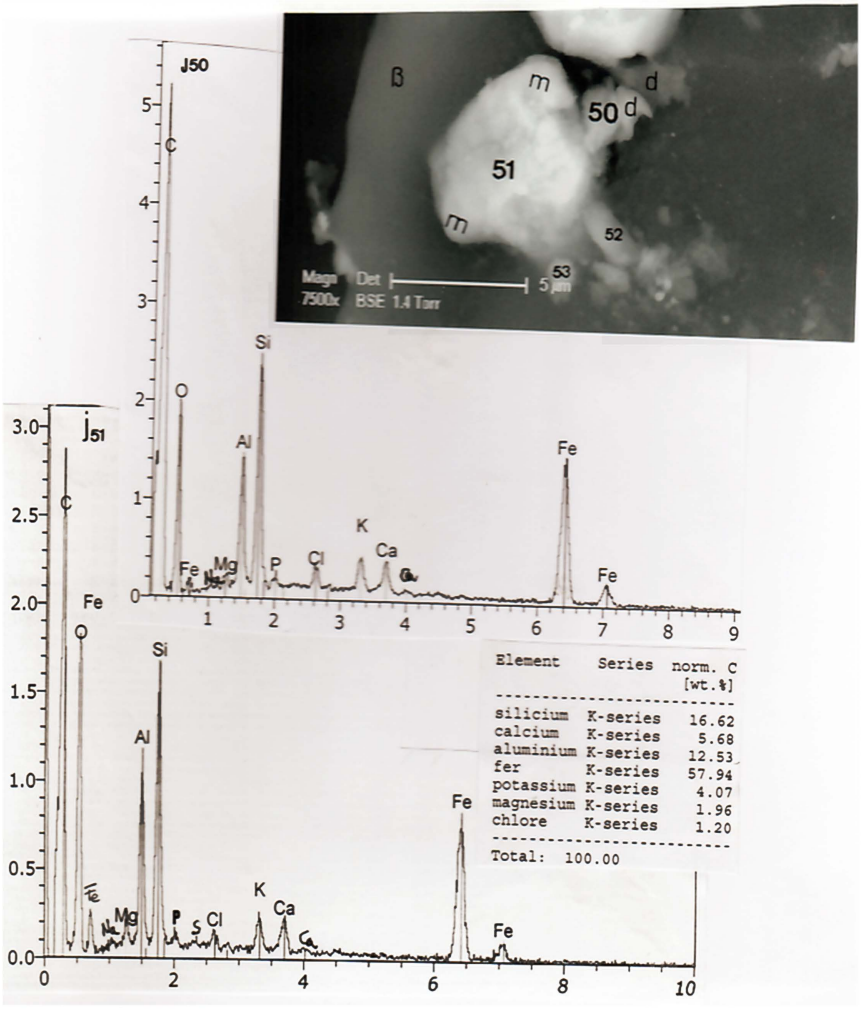

Figure 11. The j50 and j51 particles. *Above*: SEM1 photograph (7500×), in BSE, of some part of the left J area showing particles j50, and j51 with micro-organisms (m) on its surface; j48 is a spore, j49 a complex calcium carbonate, j52 a kaolinite iron-rich and j53 another clay iron-rich; B is the left border of the J area. *Upper spectrum*: the j50 spectrum. C: carbon; O: oxygen; Fe (three peaks): iron; Na: sodium; Mg: magnesium; Al: aluminium; Si: silicium; P: phosphorous; Cl: chlorine; K: potassium; Ca (two peaks): calcium. *Lower spectrum*: the HR j51 spectrum. Insert: the normal composition; (in wt.%) in elements of j50 (fer: iron; chlore: chlorine).

The forms of these particles can be rounded (a27 and b8) or more elongated (i4, j51 and l11), but most often with angular outlines. The most elementary form is that of pentagonal or hexagonal particles (a25, a27, a41, b23, b24 and b25). Two particles (g33 and j50) are squared, and one (g30) is triangular.

Table 2 summarizes the multipartism of particles, and their phosphorous and sulphur contents. There is heterogeneity in the surface of the b8 particle. Particle g27 is in seven parts. Visible micro-organisms are observed on the surfaces of the i4, j51 and l11 particles. The i4 surface (Figure 10) appears as quasi-entirely make-up of these micro-organisms, and similar patterns are observed for j51 and l11.

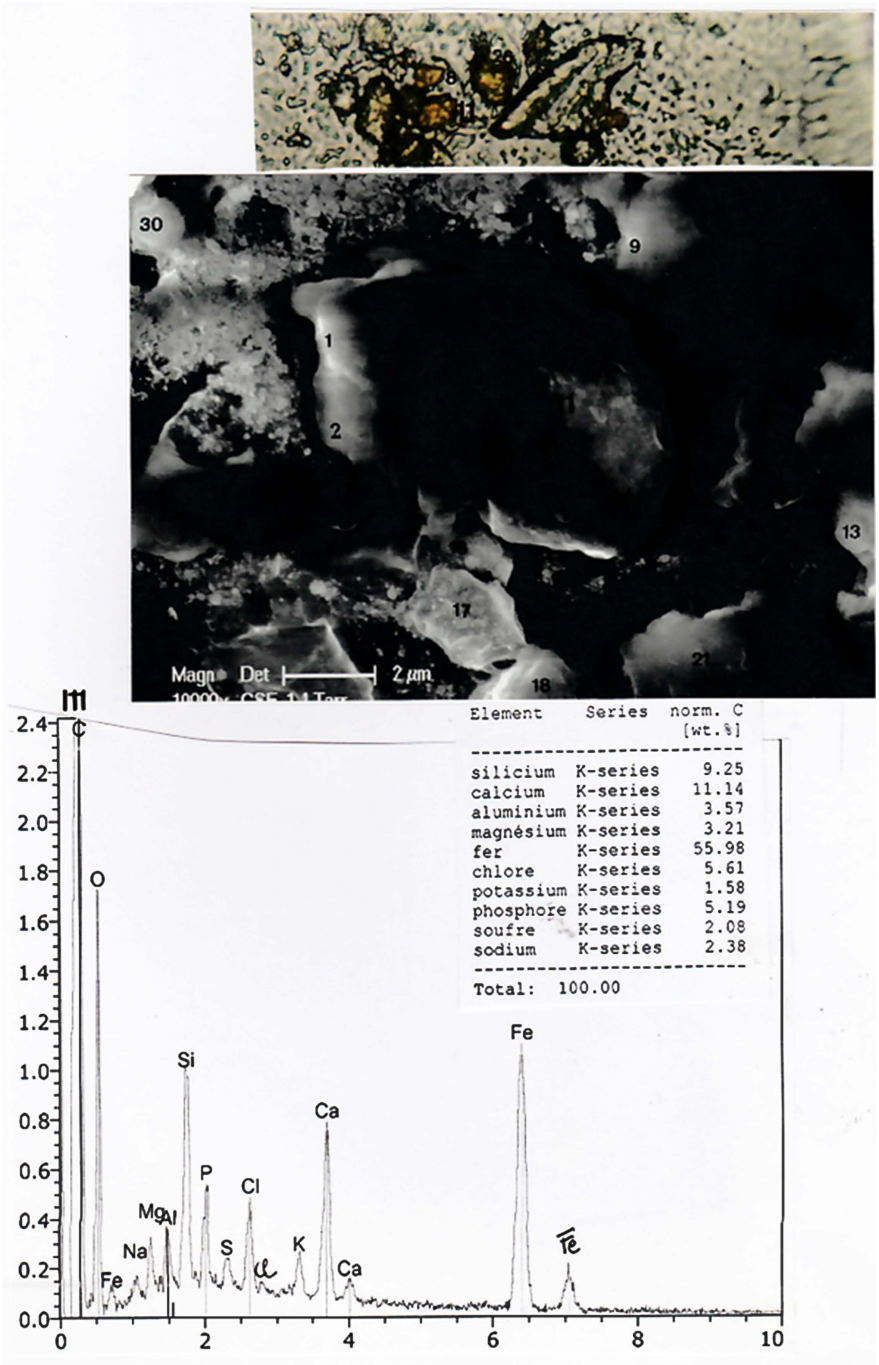

Figure 12. The l11 particle. *Upper photograph*: optical view (1200×) of some part of the L area showing the l11 particle; other red particles are l8 (an hematite particle) and l26 (a phosphorite iron particle). *Lower photograph*: SEM1 photograph (10,000×) in GSE, of some part of the L area showing the l11 particle, constituted of three parts (1, 2 and 3), and micro-organisms (m) on its surface (l16 is a Diatom, l17 a lapis-lazuli, l18 a possible citrine; l21 and l15 are PVC plastics, l13 and l30 are calcites and l25 is a gypsum). *Below*: the HR l11 spectrum. C: carbon; O: oxygen; Fe (three peaks): iron, Na: sodium; Mg: magnesium; Al: aluminium; Si: silicium; P: phosphorous; S: sulphur; Cl (two peaks): chlorine; K: potassium; Ca (two peaks): calcium. *Insert*: the normal composition (in wt. %) in elements of l11 (fer: iron; chlore: chlorine; phosphore: phosphorous; soufre: suphur).

Table 1. List and characterizations of the iron-rich clay particles detected on the various areas of the triangle.

Particle numbers	Areas of the triangle	Particles	Forms	Maximal dimensions (in µm)	Spectra of clay	Iron values	Colours	Peculiarities
1	A	a25	pentagonal	6.5 µm	+	three peaks	?	
2	A	a27	rounded	3 µm	+	three peaks	?	contaminated by titanium
3	A	a41	pentagonal	5.5 µm	+	elevated value of the main peak	red-brown	
4	B	b8	rounded	12 µm	+	41%	red	
5	B	b23	hexagonal	6 µm	+	elevated value of the main peak	?	contaminated by the Au of b22
6	B	b24	hexagonal	6 µm		three peaks	red-brown	
7	B	b25	hexagonal	6.5 µm	+	three peaks	red-brown	
8	B	b26	hexagonal	5.5 µm	+	elevated value of the main peak	?	
9	G	g27	elongated	19 µm	+	elevated value of the main peak	red-brown	contaminated by Ca
10	G	g30	triangular	3.5 µm	+	three peaks	red-brown	contaminated by Ca
11	G	g33	squared	10.5 µm	+	three peaks	red-brown	contaminated by Ca
12	I	i4	elongated	9.5 µm	+	three peaks	yellow-red point	
13	J	j50	squared	1.5 µm	+	58%	red-pale point	detached from j51
14	J	j51	elongated	7.5 µm	+	elevated value of the main peak		
15	L	l11	elongated	9 µm	+	56%	red	massively contaminated by Cl

Table 2. Multipartism of the iron-rich clays and their contents in phosphorous and sulphur.

Particle numbers	Particles	One or several parts	Phosphorous	Sulphur
1	a25	one part	traces	little peak
2	a27	one part	little peak	little peak
3	a41	one part	elevated peak	little peak
4	b8	heterogeneity	traces	1%
5	b23	one part	traces	little peak
6	b24	one part	traces	little peak
7	b25	one part	little peak	little peak
8	b26	one part	little peak	little peak
9	g27	seven parts	little peak	little peak

Continued

10	g30	one part	little peak	little peak
11	g33	one part	little peak	little peak
12	i4	visible micro-organisms inside	little peak	little peak
13	J50	one part	little peak	no
14	J51	visible micro-organisms inside	little peak	little peak
15	L11	invisible micro-organisms inside	5%	2%

All the particle spectra (but j50) have sulphur little peaks, reaching 1% in b8 and 2% in l11. All these particles have phosphorous in their spectra, most often in the form of traces (a25, b8, b23 and b24) or little peaks of this element (a27, b25, b26, g27, g30, g33, i4, j50 and j51), reaching 5% in l11.

5. Conclusion

We detected fifteen clay particles (a25, a27, a41; b8, b23, b24, b25, b26; g27, g30, g33; i4; j50, j51 and l11) on the various parts of the triangle surface. They have the following characteristics: they are particles of maximal sizes comprised between 1.5 μm (for j50) and 19 μm (for g27). Their forms are rounded or more elongated, but more often with angular outlines.

They are alumina-silicate clays, with an elevated content (up to 56% of the normal composition for particle l11) of iron; when observable, their colours are red or red-brown. Interest of these particles concerns their potential relationships to blood.

All these particles have a little quantity of the phosphorous element in their compositions (up to 5% for the particle l11). The biggest ones show some heterogeneity at their surfaces; visible micro-organisms, constitutive of these clays, are observed on the surfaces of particles i4, j51 and l11.

Conflicts of Interest

The authors declare no conflicts of interest regarding the publication of this paper.

References

Fanti, G., Galliari, I., & Canovaro, C. (2015). Analysis of Micro-Particles Vacuumed from the Turin Shroud. *Matec Web of Conferences, 36,* 1-19. https://doi.org/10.1051/matecconf/20153600001

Lucotte, G. (2012). Optical and Chemical Characteristics of the Mineral Particles Found on the Face of the Turin Shroud. *Scientific Research and Essays, 7,* 2545-2553. https://doi.org/10.5897/SRE12.383

Lucotte, G. (2015a). Exploration of the Face of the Turin Shroud. Linen Fibres Studied by SEM Analysis. *International Journal of Latest Research in Science and Technology, 4,* 78-83.

Lucotte, G. (2015b). Exploration of the Face of the Turin Shroud. Pollens Studied by SEM

Analysis. *Archaeological Discovery, 3,* 158-178. https://doi.org/10.4236/ad.2015.34014

Lucotte, G. (2015c). Red Blood Cells on the Turin Shroud. *Jacobs Journal of Hematology, 2,* 24-31.

Lucotte, G. (2016). Skin Debris on the Face of the Turin Shroud: A SEM-EDX Analysis. *Archaeological Discovery, 4,* 103-107. https://doi.org/10.4236/ad.2016.42008

Lucotte, G., Derouin, T., & Thomasset, T. (2016). Hematite, Biotite and Cinnabar on the Face of the Turin Shroud: Microscopy and SEM-EDX Analysis. *Open Journal of Applied Sciences, 6,* 601-625. https://doi.org/10.4236/ojapps.2016.69059

Lucotte, G. (2017). The Triangle Project. *Newsletter of the British Society for the Turin Shroud, 85,* 5-14.

Lucotte, G., & Thomasset, T. (2017a). Scanning Electron Microscopic Characterization and Elemental Analysis one Hair Located on the Face of the Turin Shroud. *Archaeological Discovery, 5,* 1-21. https://doi.org/10.4236/ad.2017.51001

Lucotte, G., & Thomasset, T. (2017b). An Osseous Remain on the Face of the Turin Shroud. *Journal of Anthropology and Archaeology, 5,* 30-38. https://doi.org/10.15640/jaa.v5n1a3

Lucotte, G. (2022a). Gold and Silver Particles on the Turin Shroud, Studied by Scanning Electron Microscopy and Elemental Analysis. *Archaeological Discovery, 10,* 262-281. https://doi.org/10.4236/ad.2022.104009

Lucotte, G. (2022b). SEM-EDX Characterization of the Little Clays Particles Deposited on the Turin Shroud Surface. *Journal of Multidisciplinary Engineering and Science and Technology, 10,* 15842-15847.

Lucotte, G., & Thomasset, T. (2023). Lapis Lazuli Particles on the Turin Shroud: Microscopic Optical Studies and SEM-EDX Analyses. *Archaeological Discovery, 11,* 107-132. https://doi.org/10.4236/ad.2023.112005

Marion, A., & Lucotte, G. (2006). *The Turin Shroud and Argenteuil Tunique*. Presses de la Renaissance.